Dawn/Dusk Aurora and Propagating Convection Disturbance: Ionospheric Effects of High Solar Wind Ram Pressures

X.-Y. Zhou[1], B.T. Tsurutani[1], S.B. Mende[2], H.U. Frey[2], J.F. Watermann[3], D.G. Sibeck[4], and J.K. Arballo[1]

[1]Jet Propulsion Laboratory, California Institute of Technology, Pasadena, California
[2]Space Science Laboratory, University of California, Berkeley, California
[3]Danish Meteorological Institute, Copenhagen, Denmark
[4]Applied Physics Laboratory, Johns Hopkins University, Laurel, Maryland

Submitted to AGU monograph for the LLBL New Orleans Chapman Conference, 8/20/2001

Abstract

A dawn/dusk flank auroral event has been studied using multiple observations of the WIND and POLAR spacecraft, Antactic all-sky images and Greenland magnetometers. The flank auroras were caused by a gradual ($T \approx 90$ min), intense ($P_{ram} \approx 11$ nPa) solar wind ram pressure (GISWRP) pulse that occurred on June 27, 1997. Ionospheric propagating convection disturbances were also detected within the auroras. The convection disturbance propagated antisunward at a speed of ~11 km s^{-1} which mapped with the magnetosheath flow speed very well. The auroras occurred in both diffuse and discrete forms. The energy deposition flux into discrete auroras are calculated to be increased by a factor of ~5 when the ram pressure increased by a factor of ~2 during the event. Mechanisms of the ionospheric responses are speculated to be some form of viscous interaction that occurs on the magnetopause boundary layer (such as the Kelvin-Helmholtz instability) and adiabatic compression.

1. Introduction

Dayside auroral onset and evolution have been found to be closely related to the solar wind ram pressure (ρV^2) variation. Shock-auroras occur with onsets near local noon and propagate antisunward along the auroral oval when interplanetary shocks compress the dayside magnetopause (Craven et al., 1986; Arballo et al., 1998; Spann et al., 1998; Zhou and Tsurutani, 1999; Brittnacher et al., 2000). The suggested mechanisms for the particle precipitation are adiabatic compression and field-aligned current enhancement (Zhou and Tsurutani, 1999; Tsurutani et al., 2001).

Zhou and Tsurutani (2001) have also shown that dawn and dusk flank auroras increase (decrease) linearly with solar wind ram pressure gradual increases (decreases). The suggested mechanism is some form of viscous interaction occurring on the magnetopause flanks, such as the Kelvin-Helmholtz (K-H) instability (Zhou and Tsurutani, 2001). Since the magnetopause and magnetosphere are also compressed severely when the solar wind pressure increases to high values ($P_{ram} \geq 10$ nPa), the mechanisms for shock-auroras may also apply to the flank auroras (i.e., pitch angle scattering and magnetic field shearing could also occur).

It has been reported that solar wind pressure variations can cause magnetopause surface waves (Song et al., 1988; Sibeck et al., 1989; Southwood and Kivelson, 1990), ground magnetic Pc pulsations (Olsen and Rostoker, 1978; Wolfe et al., 1987), and ionospheric traveling vortices (Friis-Christensen et al., 1988). Suggested mechanisms for those phenomena are the K-H instability (Miura 1984, 1992; McHenry et al., 1990; Kivelson and Southwood, 1991), the magnetic reconnection (Lanzerotti et al., 1986), and IMF B_y variations (Lee, 1986; Southwood,

1987; McHenry and Clauer, 1987; Stauning, 1995). However, whether auroras will occur accompanying Pc pulsations and/or the traveling vortices and what is the mechanism when auroras occur are still not well understood.

In this paper, we will study a dawn/dusk flank auroral event using multiple observations. We will show auroral variations in a global view by POLAR UVI data, and auroral micro-structures by ground-based all-sky imager (ASI) data. Greenland magnetometer data will show ionospheric convection structure within the auroras. Mechanisms for the flank auroras will be discussed.

2. Observations of June 27, 1997 Event

In this section, we will show multiple observations for a solar wind-magnetosphere-ionosphere interaction event caused by gradual, intense solar wind ram pressure pulse (GISWRP). WIND magnetic field and plasma data (Lepping et al., 1995; Ogilvie et al.,1995) are used to show the increase GISWRP event. POLAR UVI data (Torr et al., 1995) show the auroral response (on north pole) to the pressure increase. Antarctic ASI data (Rosenberg and Doolittle, 1994) of stations P2 and SPA (South Pole) are used to analyze the auroral forms. Greenland magnetometer data (Friis-Christensen et al., 1985) are used to identify the ionospheric convection.

In this study, by "flank auroras" we mean auroras that occur on dawnside within ~03-09 magnetic local time (MLT), and on duskside within ~15-21 MLT. We assume that the auroral conjugacy existed for this event due to the global effect of this intense pressure pulse (which will be discussed later).

2.1 Interplanetary conditions

On June 27 1997, during 0730-0910 UT, the WIND spacecraft was located in the upstream solar wind at (81, 14, -11R_E) in the GSM coordinates. The time delay for the solar wind to propagate from WIND to the nose of the magnetopause (assuming at 10 R_E) was ~20 min. Figure 1 shows WIND observations of the interplanetary magnetic field (IMF) magnitude (B), three components in GSM coordinates (B_x, B_y and B_z) and solar wind proton density (N_p), speed (V_{sw}) and ram pressure (P_{ram}) for this specific duration. The solar wind parameters have been shifted 20 min due to the time delay. The shifted time is displayed on the bottom of Figure 1. The time on the top is the one without time shifting. We will use the bottom time to describe the solar wind conditions for the sake of later comparison with the POLAR UVI and ground-based observations.

Figure 1 shows that the IMF magnitude was ~6 nT during the whole event until a sudden increase to ~12 nT at ~0930 UT. The IMF B_x component was slight negative at ~-2 nT before 0900 UT, then changed to positive and reached at ~4 nT at ~0915 UT. The B_y component changed suddenly from positive to negative at ~0828 UT and mainly stayed at the dawn direction afterwards. The IMF B_z turned to southward from slight northward at ~0813 UT and was at ~-7 nT from ~0823 to 0850 UT. It mainly remained northward after 0900 UT until suddenly turned to southward from ~6 to -10 nT at 0930 UT when the IMF magnitude suddenly increased. The solar wind proton density began to increase slowly from ~15 cm^{-3} at ~0800 UT and reached a maximum ~35 cm^{-3} at ~0930 UT, the density decreased sharply together with the occurrence of the magnetic field discontinuity. The solar wind speed increased from ~380 km s^{-1}

at ~0800 UT to ~400 km s^{-1} at ~0830 UT. Then the speed was stable at this level at the rest time of this event. The solar wind ram pressure began to increase slowly from ~0800 UT with the density increases. At ~0800 UT the pressure was ~5 nPa, at ~0915 UT the pressure increased to a maximum value ~11 nPa, and it remained at this value until a sudden decrease at ~0930 UT.

2.2 Auroral response detected from space by POLAR UVI

Figure 2 shows the north pole auroral response to the above GISWRP event. Greenland outlines and the conjugated locations of Antarctic stations are superposed onto the left column of Figure 2 for the later comparison with ground-based ASI and magnetometer data. At 0804:40 UT, when the solar wind pressure was ~4.5 nPa, there was faint dawn and dusk auroras which was related to the previous interplanetary conditions and magnetospheric/ionospheric responses. The auroral intensities at 0600 MLT (magnetic local time) was ~23 photons cm^{-2} s^{-1}, at 1800 MLT was ~20 photons cm^{-2} s^{-1}. Afterward, the flank auroral intensity increased gradually. At 0841:28 UT, when the pressure was at ~6 nPa, the auroral intensities at 0600 MLT was ~35 photons cm^{-2} s^{-1}, and was ~27 photons cm^{-2} s^{-1} at 1800 MLT. Within this duration (0804-0841 UT), the aurora in the 0600-0900 MLT sector was mainly in a high latitude region of ~69°-78° MLAT (magnetic latitude).

From 0858:38 UT, the flank auroral intensity and shape became more or less symmetric with the noon and midnight meridional line. But duskside oval was higher (~2° MLAT) and more narrow in the latitudinal direction than the dawnside oval. At 0904:46 UT when the pressure was ~9 nPa, the dawn (at 06 MLT) and dusk (18 MLT) auroral intensities were at about the same level at ~60 photons cm^{-2} s^{-1}. From 0907:50 UT, nightside auroral activities began to increase,

but mainly in the 2000-0000 MLT sector. So the dawnside aurora was not contaminated by this nightside auroral activity. The dawnside (at 06 MLT) auroral intensities increased to a peak value of ~100 photons cm^{-2} s^{-1} at 0929:18 UT. At this time the solar wind pressure was ~11 nPa. The last two images of Figure 2 show that the dawnside auroral intensities decreased significantly. This decrease was consistent with the pressure sudden decrease (at the IMF discontinuity) that occurred at ~ 0930 UT (see Figure 1, bottom panel).

2.3 Auroral response detected from ground by ASIs

During this event, the GEOTAIL spacecraft was at (15, 21, -2 R_E) in the GSE coordinates and detected the same IMF and solar wind pressure structure (not shown) as WIND detected in further upstream solar wind. The INTERBALL-TAIL spacecraft was located immediately upstream from the subsolar bow shock and detected the antisunward ion flux increased from 7.0×10^8 cm^{-2} s^{-1} at ~0800 UT to 1.6×10^9 cm^{-2} s^{-1} at ~0920 UT. So we can expect this GISWRP event was in big spatial region that would compress the whole Earth magnetosphere. Furthermore, the auroral response (in Figure 2) have shown to be a global effect. Therefore, we assume that the auroral conjugacy existed during this event. We, then, use south pole ASI data to show the auroral micro-structure within the global UV images.

The ASI data of two U.S. AGO (Automatic Geophysical Observatories) stations are used in this study. One is SPA (South Pole Station), at (-74.0°, 18.4°) in CGM (Corrected GeoMagnetic) coordinates. Another is P2 at (-69.8°, 19.3°). So the two stations are at approximately the same magnetic local time, with 4° MLAT apart from each other. The imagers at each station is capable of acquiring images in two different wavelengths (the red line on 630.0 nm and the blue line on

427.8 nm) simultaneously (Rosenberg and Doolittle, 1994). Image data, recorded at a rate of one image every 2 minutes in general, have 10 km geographic resolution over most of the field of view, ranging to 30 km at the edges. The emission in 630.0 nm comes from 200-250 km with the useful horizontal range at 500 km in radius. The emission in 427.8 nm comes from ~ 110 km altitude with a field of view in 300 km radius.

Figure 3 shows ASI data of SPA (the top three rows) and P2 (the bottom three rows) from 0800 to 0950 UT with 10 min resolution. The auroral intensity changed gradually within this duration. There are two images in each frame. For each image, the top points to the geomagnetic pole in the southern hemisphere, the right to the east. For SPA station, the left image is the red emission at 630.0 nm wavelength and the right one is the blue emission at 427.8 nm. The exposure was 1.8 sec. For P2 station, the blue emission is on left, the red emission is on right. The exposure was 16 sec. The bright spots in the background of each frame is a calibration light source.

From 0800 to 0930 UT, SPA and P2 were located within ~0430 to 0600 MLT. The SPA station was at the poleward edge of the auroral oval during the event. The conjugated locations of SPA (the circle) and P2 (the asterisk) are shown in the left column of Figure 2. During whole event the auroral emission was mainly the red emission at 630.0 nm. Arcs were detected in the middle of the sky at 0800 UT and moved equatorward at 0810 UT. From 0820 to 0900 UT, only faint auroras occurred on the southern rims of the images indicating there were auroras at lower latitudes. After 0910 UT, the lighted southern rim became wider and brighter. The auroral brightening reached a maximum at 0929 UT (not shown) when the solar wind ram pressure

reached the maximum value of ~11nPa. With the 10 min cadence, the image at 0930 UT shows the brightest aurora. The above processes also indicated that lower latitude auroras were getting brighter and expanded into higher latitudes. At 0940 and 0950 UT, the auroras at the southern rims decreased gradually due to the auroras at lower latitudes were decaying.

The P2 station, which is ~4° MLAT lower than SPA, was close to the latitudinal center of the auroral brightening as shown in Figure 2. At P2 the 427.8 nm blue emission is on left and the 630.0 nm red emission is on right. Before 0800 UT there were more diffuse auroras in the blue emissions. At 0810 UT, arcs occurred in the middle of the sky along the oval, i.e., east-west direction, in both emissions. The arcs moved equatorward as seen in the images from 0810 to 0840 UT. At 0850 UT, very bright diffuse auroras occurred in the 427.8 nm emission in south-east sky and expanded towards west and south at 0900 UT, while in the 630.0 nm emission a thick and bright auroral arc occurred in middle and south sky and moved equatorward as it became blurry at 0900 UT. From 0910 to 0930 UT, bright diffuse auroras became very intense filled in the half sky on east and south in the 427.8 nm emissions. The auroral intensity in the 630.0 nm emissions increased and reached a maximum at 0930 UT. It should note that the solar wind ram pressure increased to a maximum value of ~11 nPa during this time. The auroral brightening decreased after 0930 UT (as shown in the images at 0940 and 0950 UT) when the solar wind pressure decreased.

Energy deposition has been calculated Rees and Luckey model (1974) for the discrete auroras detected by SPA. Arrows have been added into the images at 0830, 0900 and 0930 UT to show the arcs used for the calculation. The calculation has not been done for the P2 data because

the images were overexposed. After the correction for the Van Rhijn effect (Chamberlain, 1961), the calculation results are listed in Table 1. In the table, α is the characteristic energy of the Maxwellian distribution, f_e is the total number, f_E is the corresponding energy flux ($f_E = 2\alpha f_e$). By "East", we mean the eastern arc; by "North", we mean the northern (equatorward) arc. These results show that the energy deposition into the discrete auroras at the SPA station region increased by a factor of ~5 (on average) from 0830 to 0930 UT when the solar wind ram pressure increased by a factor of ~2 from ~5.5 to 11 nPa.

Table 1. Energy deposition into the discrete auroras.

Red Emission	α keV	f_e $\times 10^8$ electrons cm^{-2} s^{-1}	f_E ergs cm^{-2} s^{-1}
		0830 UT	
East	0.6	1.0	0.19
North	1.5	1.5	0.72
		0900 UT	
East	0.4	2.0	0.26
North	3.0	1.7	1.6
		0930 UT	
East	1.2	5.0	1.9
North	2.0	4.0	2.6

2.4 Greenland magnetometer observations.

Greenland magnetometer chain was at dawn during this event. From 0800 to 0930 UT, both west and east coast chains covered a region from ~0500 to 1200 MLT (as shown in Figure 2). Figure 4a shows a map of Greenland stations with dot lines for geographic latitudes (from 60° to 80°) and longitudes, and dashed lines for CGM latitudes (from 65° to 85°). Figure 4b is North-component stack plot with west coast stations on the top part and east coast stations on the

bottom part. A Kaiser-Bessel filter (Openheim et al., 1999), applied in the time domain, with 3-30 min band-pass was used on the data to remove the Earth's background field and the higher frequency noise at the KUV station.

In Figure 4b, propagating convection disturbances were detected by the Greenland magnetometers when the solar wind pressure began to increase from ~0800 UT. But the disturbances were only occurred at high latitude stations. These stations cover a latitudinal region from ~72° (the SKT station) to 81° (the NRD station) MLAT, which maps into the low latitude boundary layer (LLBL) (McHenry et al., 1990). The magnetic fluctuation has a period of ~20 min with amplitudes at ~40 nT.

To determine the convection disturbance propagating speed, one can divide the distance between the west and east coast chains by the time difference of correlated observations at these two positions. The west coast station UMQ (77.0°, 43.9° CGM) and the east coast station DMH (77.3°, 87.1° CGM) were used for this calculation. The two stations are approximately at the same magnetic latitude and marked by asterisks in Figure 4b. Two vertical solid lines were drawn at the peaks of the fluctuations detected by UMQ at ~0817 and 0838 UT, respectively. The similar signatures were detected by DMH at ~2 min prior to the detection at UMQ. The two stations are approximately 1300 km apart, hence the speed was at ~11 km s^{-1} and moving antisunward.

By using Petrenic and Russell magnetopause model (1996) and the solar wind parameters with P_{ram} = 6 nPa, IMF B_z = -7 nT at ~0830 UT, the calculated magnetopause location at 0600

MLT was ~12 R_E. Mapping the propagating speed of ~11 km s^{-1} in the ionosphere into the dawnside magnetopause (by the same angular speed) at 12 R_E, we obtained the magnetosheath speed at ~405 km s^{-1}. At 0830 UT, the solar speed at the GEOTAIL spacecraft and was ~390 km s^{-1}, which is very close to the calculated magnetosheath speed.

3. Observation Summary

In Section 2 we have presented an event of ionospheric responses to an increase GISWRP event. On June 27, 1997, from ~0800 to 0930 UT, the solar wind pressure increased from ~4 to 11 nPa. Auroral borealis observed by POLAR UVI increased mainly on both dawn and dusk auroral oval flanks. The intensities increased from ~23 to 100 photons cm^{-2} s^{-1} near 0600 MLT and ~20 to 50 photons cm^{-2} s^{-1} near 1800 MLT. On the Antarctic SPA and P2 stations, diffuse and discrete auroras were detected at ~0500-0600 MLT of the auroral oval latitude on both emissions of 630.0 nm and 427.8 nm. The energy deposition rate into discrete auroras at the SPA station increased by a factor of ~5 from 0830 to 0930 UT.

Greenland magnetometer chain was at ~0500-1200 MLT during the event. Propagating convection disturbances were detected from ~0800 to 1000 UT by high latitude stations (72°-80° MLAT) which map to the LLBL. The disturbances propagated antisunward at a speed of ~ 11 km s^{-1}, which matched very well with the magnetosheath flow speed.

4. Discussion and Conclusion

In this study, we have shown that ionospheric propagating convection disturbances occurred at dawnside 72°-80° MLAT region when the solar wind ram pressure increased gradually to

intense values. Similar phenomena have been reported by McHenry and Clauer (1987). Although the IMF B_z turned to southward at ~0813 UT and to northward at ~0902 UT, there were no obvious effects in the geomagnetic fields and the auroral intensities. It is more likely that the ionospheric convection disturbances were caused by the solar wind pressure increase.

Comparing Figure 2 and 4, it is interesting to note that auroras occurred at high latitude region where propagating convection disturbances were intense during the time ~0800-0850 UT. The auroras covered an area from ~69° to 78° MLAT in the ~0600-0900 MLT sector. The propagating convection disturbances detected by the Greenland stations were located within 72° - 80° MLAT region in the same local time sector. The spatial overlap between the auroras and convection disturbances indicates that both of them could have been caused by LLBL disturbances.

For the first time, we have shown that flank auroras caused by GISWRP event are related to ionospheric propagating convection disturbances. Unfortunately, there was no LLBL observations for the June 27, 1997 event. So we couldn't be aware of what kind disturbances had occurred on the magnetopause boundary layer. McHenry et al. (1990) have shown that ionospheric traveling vortices can be caused by the K-H instability on the magnetopause flanks. If K-H instability occurred during this event, one would expect vortical flows could occur on the magnetopause boundary layer (Sibeck, 1990). These flows may drive a guided shear wave into the ionosphere and excite a pair of field-aligned currents (Kivelson and Southwood, 1991). One speculation is that particles pre-existing in the outer magnetosphere or transferred from the magnetosheath into the magnetosphere during the K-H instability (Nykyri and Otto, 2001) might

be accelerated along the field-aligned currents and precipitated into the ionosphere. This scenario predicts that discrete auroras could occur in the ionosphere at the magnetic latitudes which map to the LLBL.

There was no ground ASI observations at Greenland because of the season to show whether there was auroral arcs in this region. But we have shown in Figure 3 that the auroral arcs had been detected by the ASIs at the SPA and P2 stations. It should be noted that similar geomagnetic disturbances were detected by the magnetometer at SPA (not shown in this paper). But at P2, a negative bay with amplitude at ~100 nT was detected at ~0830 UT indicating a westward current above P2 along the auroral oval.

From ~0850-0910 UT when the solar wind ram pressure increased intensely from ~6 to 10 nPa and the IMF B_z turned to northward from ~-5 to 0 nT. The auroral oval became narrow in the latitudinal direction, especially on the dawnside (Figure 2). The whole oval became brighter and moved to lower geomagnetic latitude except the noon sector. During this period, the calculated magnetopause flank locations moved inward from ~12.3 to 11.3 R_E. This intense magnetopause compression could lead to particle recipitation via the loss-cone instability and cause diffuse auroras. This is also one of possible mechanisms for shock-auroras (Zhou and Tsurutani, 1999).

In this paper, we have shown that dawn and dusk flank auroras caused by a GISWRP event can be in both diffuse and discrete formats and be propagating convection disturbance related. The mechanisms for the reported phenomena has been speculated to be some form of viscous

interaction on the magnetopause, such as the K-H instability. Adiabatic compression could be another possible mechanism to cause particle precipitate into the ionosphere when the magnetopause and outer magnetosphere were severely compressed.

Acknowledgements: Portions of this research were performed at the Jet Propulsion Laboratory, California Institute of Technology, Pasadena, under contract with NASA.

References

Arballo, J.K., C.M. Ho, B.T. Tsurutani, X.-Y. Zhou, Y. Kamide, J.-H. Shue, S.-I. Akasofu, R.P. Lepping, C.C. Goodrich, K. Papadopoulos, A.S. Sharma and J.G. Lyon, Pseudobreakups during January 10, 1997, in *Substorms-4*, edited by S. Kokubun and Y. Kamide, Terra Sci. Publ., 315-318, 1998.

Brittnacher, M., M. Wilber, M. Fillingim, D. Chua, G. Parks, J. Spann, and G. Germany, Global auroral response to a solar wind pressure pulse, *Adv. Space Res.* 25, 1377, 2000.

Chamberlain, J.W., Physics of the airglow and aurora, Academic Press, New York, 1961.

Craven, J.D., L.A. Frank, C.T. Russell, E.E. Smith, and R.P. Lepping, Global auroral responses to magnetospheric compressions by shocks in the solar wind: Two case studies, in *Solar Wind-Magnetosphere Coupling*, edited by Y. Kamide and J.A. Slavin, pp. 367-380, Terra Scientific, Tokyo, 1986.

Friis-Christensen, E., Y. Kamide, A.D. Richmond, and S. Matsushita, Interplanetary magnetic field control of high-latitude electric fields and currents determined from Greenland agnetometer data, *J. Geophys. Res., 90*, 1325, 1985.

Friis-Christensen, E., M.A. McHenry, C.R. Clauer, and S. Vennerstrom, Ionospheric traveling convection vortices observed near the polar cleft; A triggered response to sudden changes in the solar wind, *Geophys. Res., Lett., 15*, 253, 1988.

Kivelson, M.G., and D.J. Southwood, Ionospheric traveling vortex generation by solar wond buffeting of the magnetosphere, *J. Geophys. Res., 96,* 1661, 1991.

Lanzerotti, L.J., L.C. Lee, C.G. Maclennan, A. Wolfe, and L.V. Medford, Possible evidence of flux transfer events in the polar ionosphere, *Geophys. Res. Lett., 13*, 1089, 1986.

Lee, L.C., Magnetic flux transfer at the Earth's magnetopause, *Solar Wind-Magnetosphere Coupling*, edited by Y. Kamide and J.A. Slavin, pp. 297-314, Terra, Tokyo, 1986.

Lepping, R.P., M.H., Acuna, L.F. Burlaga, W.M. Farrell, J.A. Slavin, K.H. Schatten, F. Mariani, N.F. Ness, F.M. Neubauer, Y.C. Whang, J.B. Byrnes, R.S. Kennon, P.V. Panetta, J. Scheiffle, and E.M. Worley, The WIND magnetic field investigation, *Space Sci. Rev., 71,* 207, 1995.

McHenry, M.A., and C.R. Clauer, Modeled ground magnetic signatures of flux transfer events, *J. Geophys. Res., 92,* 11231, 1987.

McHenry, M.A., C.R. Clauer, E. Friss-Christense, PlT. Newell, and J.D. Kelly, Ground observations of magnetospheric boundary layer phenomena, *J. Geophys. Res., 95,* 14995, 1990.

Mirua, A., Anomalous transport by magnetohydrodynamic Kelvin-Helmholtz instabilities in the solar wind - magnetosphere interaction, *J. Geophys. Res., 89*, 801, 1984.

Miura, A., Kelvin-Helmholtz instability at the magnetospheric boundary: dependence on the magnetosheath sonic Mach number, *J. Geophys. Res., 97*, 10655, 1992.

Nykyri, K. and A. Otto, Plasma transport at the magnetospheric boundary due to reconnection in Kelvin-Helmholtz vortices, *Geophys. Res. Lett.,* in press, 2001.

Ogilvie, K.W., D.J. Chornay, R.J. Fritzenreiter, F. Hunsaker, J. Keller, J. Lobell, G. Miller, J.D. Scudder, E.C. Sittler, Jr., R.B. Torbert, D. Bodet, G. Needell, A.J. Lazarus, J.T. Steinberg, J.H. Tappan, A. Mavertic, and E. Gergin, SWE, A comprehensive plasma instrument for the WIND spacecraft, *Space Sci. Rev., 71,* 55, 1995.

Olson, J.V., and G. Rostoker, Longitudinal phase variations of Pc 4-5 micropulsations, *J. Geophys. Res., 83*, 2481, 1978.

Openheim, A.V., R.W. Schafer and J.R. Buck, Discrete-Time Signal Processing, 2nd ed., Prentice Hall, Inc., Engelwood Cliffs, N.J., 1999.

Petrinec, S.M., and C.T. Russell, Near-Earth magnetotail shape and size as determined from the magnetopause flaring angle, *J. Geophys. Res.,* 101, 137, 1996.

Rees, M.H., and D. Luckey, Auroral electron energy derived from fatio of spectroscopic emissions 1. Model computations, *J. Geophys. Res., 79*, 5181, 1974.

Rosenberg, T.J. and J.H. Doolittle, Studying the polar ionosphere and magnetosphere with Automatic Geophysical Observatories: The U.S. program in Antarctica, *Antarctic Journal of the United States, 29*, 347, 1994.

Sibeck, D.G., W. Baumjohann, R.C. Elphic, D.H. Fairfield, J.F. Fennell, W.B. Gail, L.J. Lanzerotti, R.E. Lopez, H. Luehr, L.T.Y. Lui, C.G. Maclennan, R.W. McEntire, T.A. Potemra, T.J. Rosenberg, and K. Takahashi, The magnetospheric response to 8-minute-period strong-amplitude solar wind pressure variations, *J. Geophys. Res., 94,* 2505, 1989.

Sibeck, D.G., A model for the transient magnetospheric response to sudden solar wind dynamic pressure variations, *J. Geophys. Res., 95,* 3755, 1990.

Song, P., R.C. Elphic, and C.T. Russell, ISEE 1 and 2 observations of the oscillating magnetopause, *Geophys. Res. Lett., 15*, 744, 1988.

Southwood, D.J., The ionospheric signature of flux transfer events, *J. Geophys. Res., 92,* 3207, 1987.

Southwood D.J., and M.G. Kivelson, The magnetohydrodynamic response of the magnetospheric cavity to changes in solar wind pressure, *J. Geophys. Res., 95*, 2301, 1990.

Spann, J.F., M. Brittnacher, R. Elsen, G.A. Germany, and G.K. Parks, Initial response and complex polar cap structures of the aurora in response to the January 10, 1997 magnetic cloud, *Geophys. Res. Lett., 25*, 2577, 1998.

Stauning, P., Progressing IMF By-related polar ionospheric convection disturbances, *J. Geomagn. Geoelectr., 47*, 735, 1995.

Torr, M.R., D.G. Torr, M. Zukic, R.B. Johnson, J. Ajello, P. Banks, K. Clark, K. Cole, C. Keffer, G. Parks, B. Tsurutani, and J. Spann, A far ultraviolet imager for the international solar-terrestrial physics mission, *Space Sci. Rev.*, *71*, 329, 1995.

Tsurutani, B.T., X.-Y. Zhou, J.K. Arballo, W.D. Gonzalez, G.S. Lakhina, V. Vasyliunas, J.S. Pickett, T. Araki, H. Yang, G. Rostoker, T.J. Hughes, R.P. Lepping, and D. Berdichevsky, Auroral zone dayside precipitation during magnetic storm initial phases, *J. Atmos. Solar-Terr. Phys.*, *63*, 513, 2001.

Wolfe, A., E. Kamen, L.J. Lanzerotti, C.G. MacLennan, J.F. Bamber, and D. Venkatesan, ULF geomagnetic power at cusp latitudes in response to upstream solar wind conditions, *J. Geophys, Res., 92,* 168, 1987.

Zhou, X.-Y., and B.T. Tsurutani, Rapid intensification and propagation of the dayside aurora: Large scale interplanetary pressure pulses (fast shocks), *Geophys. Res. Lett.*, *26*, 1097, 1999.

Zhou, X.-Y., and B.T. Tsurutani, Dawn and dusk auroras caused by gradual, intense solar wind ram pressure (GISWRP) events, submitted to *Geophys. Res. Lett.*, 2001.

Figure Captions

Figure 1. A pressure increase GISWRP event on June 27, 1997, detected by the WIND spacecraft at (81, 14, -11 R_E) in the GSM coordinates.

Figure 2. The auroral response for the GISWRP event shown in Figure 1. The auroras were observed by POLAR UVI with LBH-long filter centered at ~170.0 nm (for molecular nitrogen lines). The image cadence is ~3 min with time sequence goes from left to right and down. For every image, geomagnetic coordinates are used with the magnetic pole at the center, noon on the top and dawn on right. The conjugate positions of SPA (the circle) and P2 (the asterisk) are denoted in the left column of the images.

Figure 3. Ground-based observations for the GISWRP event shown in Figure 1. The ASI data are of SPA (the top three rows) and P2 (the bottom three rows). Two emissions at 630.0 nm (red) and 427.8 nm (blue) wavelength were recorded by the ASIs. The images are shown by the red emission on left, the blue on right at SPA, but it is vice versa at P2.

Figure 4. (a) a map of Greenland magnetometer station and (b) stack plot of geomagnetic North-component with west coast data above the AMK plot, and east coast data below the AMK. A Kaiser-Bessel filter with 3-30 min band-pass has been applied on the data.

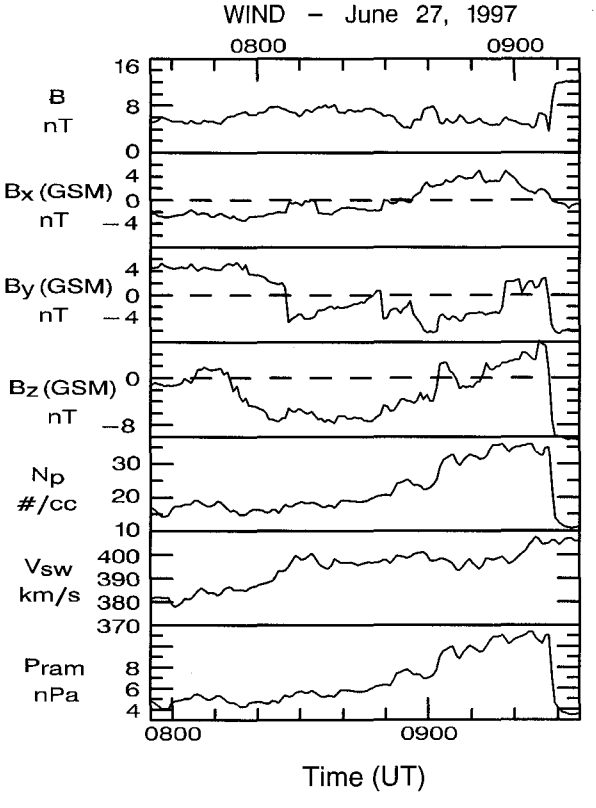
WIND – June 27, 1997
0800
0900
B
nT
16
8
0
Bx (GSM)
nT
4
0
−4
By (GSM)
nT
4
0
−4
Bz (GSM)
nT
0
−8
Np
#/cc
30
20
10
Vsw
km/s
400
390
380
370
Pram
nPa
8
6
4
0800
0900
Time (UT)

Figure 1

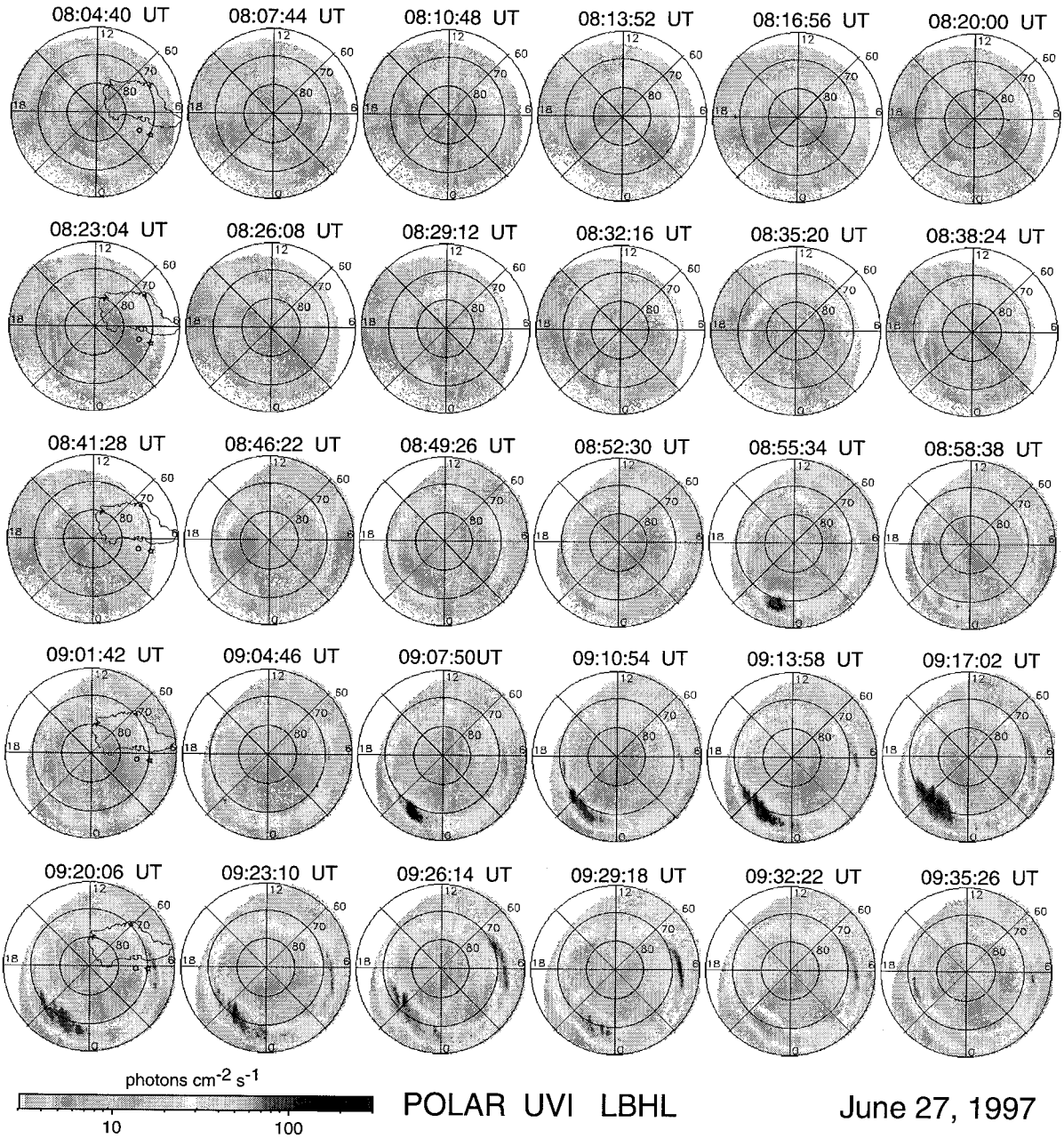
08:04:40 UT
08:07:44 UT
08:10:48 UT
08:13:52 UT
08:16:56 UT
08:20:00 UT
08:23:04 UT
08:26:08 UT
08:29:12 UT
08:32:16 UT
08:35:20 UT
08:38:24 UT
08:41:28 UT
08:46:22 UT
08:49:26 UT
08:52:30 UT
08:55:34 UT
08:58:38 UT
09:01:42 UT
09:04:46 UT
09:07:50UT
09:10:54 UT
09:13:58 UT
09:17:02 UT
09:20:06 UT
09:23:10 UT
09:26:14 UT
09:29:18 UT
09:32:22 UT
09:35:26 UT
photons cm-2 s-1
10
100
POLAR UVI LBHL
June 27, 1997

Figure 2

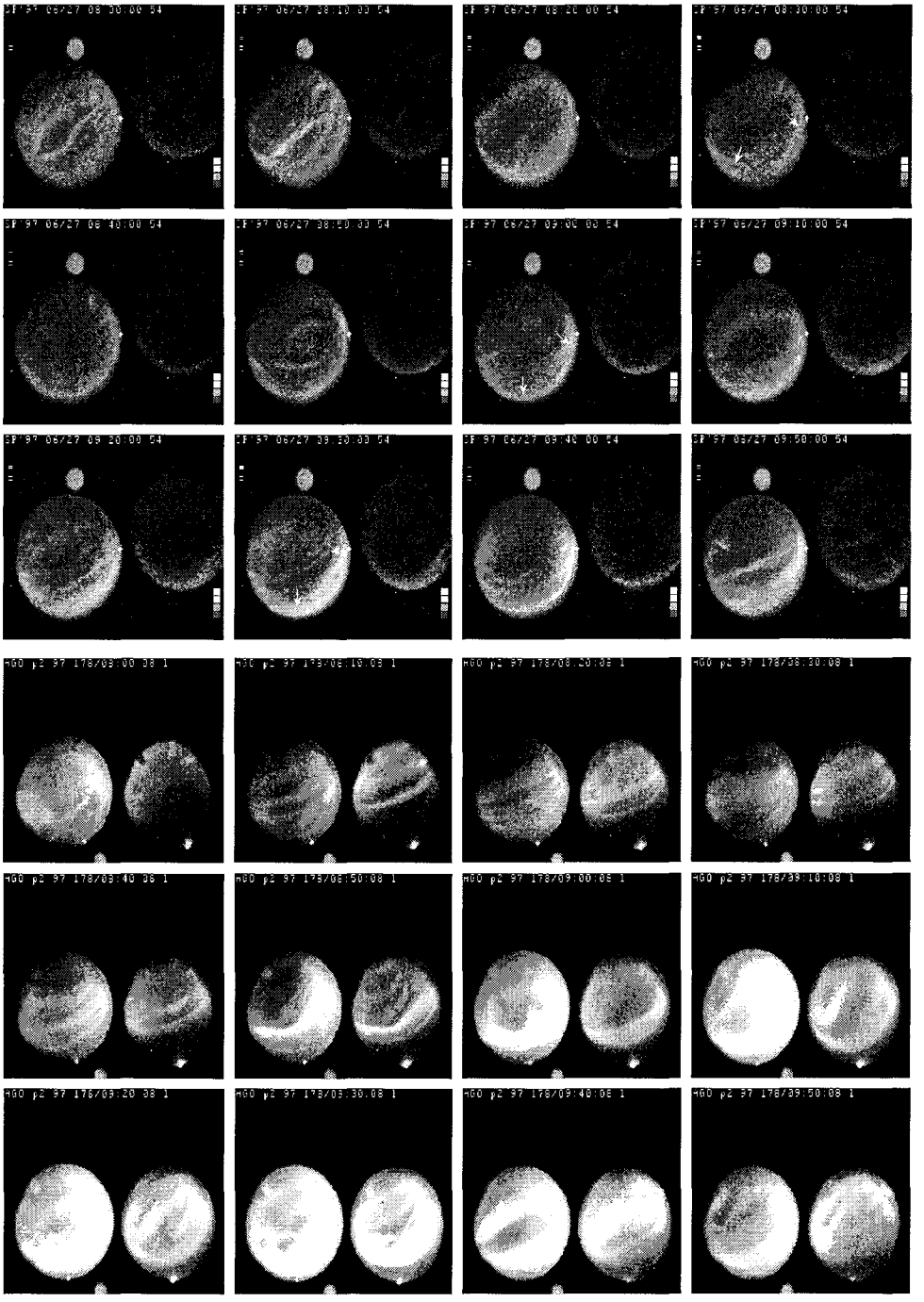

Figure 3

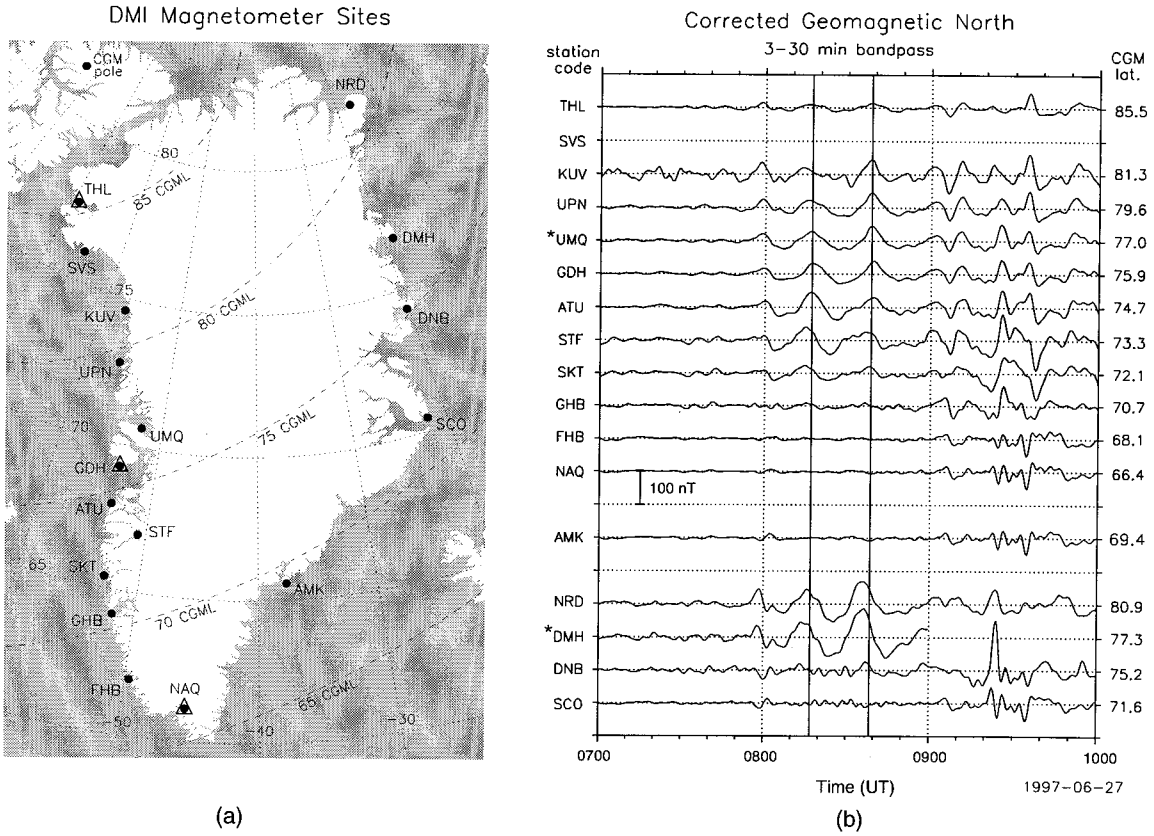
DMI Magnetometer Sites
CGM pole
NRD
80
THL
85 CGML
DMH
SVS
75
KUV
80 CGML
DNB
UPN
70
UMQ
75 CGML
SCO
GDH
ATU
STF
65
SKT
AMK
GHB
70 CGML
FHB
NAQ
65 CGML
−50
−40
−30
(a)
Corrected Geomagnetic North
station code
3–30 min bandpass
CGM lat.
THL
85.5
SVS
KUV
81.3
UPN
79.6
*UMQ
77.0
GDH
75.9
ATU
74.7
STF
73.3
SKT
72.1
GHB
70.7
FHB
68.1
NAQ
66.4
100 nT
AMK
69.4
NRD
80.9
*DMH
77.3
DNB
75.2
SCO
71.6
0700
0800
0900
1000
Time (UT)
1997-06-27
(b)

Figure 4